Dynamic Management Zones for Irrigation Scheduling

Mireia Fontanet [1,2,3], Elia Scudiero [4,5], Todd H. Skaggs[5], Daniel Fernàndez-Garcia [2,3], Francesc Ferrer [1], Gema Rodrigo [1], Joaquim Bellvert [6]

[1] LabFerrer, Cervera, 25200, Spain

[2] Department of Civil and Environmental Engineering, Universitat Politècnica de Catalunya (UPC), Barcelona, 08034, Spain

[3] Associated Unit: Hydrogeology Group (UPC-CSIC)

[4] Department of Environmental Sciences, University of California Riverside, 900 University Ave., Riverside, CA 92521, USA

[5] USDA-ARS, United States Salinity Laboratory, 450 West Big Springs Rd., Riverside, CA 92507, USA

[6] Efficient Use of Water in Agriculture Program, Institute of Agri-Food, Research and Technology (IRTA), Fruitcentre, Parc Científic i Tecnològic de Gardeny, 25008, Lleida, Spain

Highlights

- We used Sentinel 2 NDVI time-series to delineate dynamic management zones (MZ)
- Changes in MZ patterns were consistent with soil moisture spatiotemporal variability
- Data variance fragmentation was used for daily evaluation of the dynamic MZ designs
- Soil moisture data and model forecasts can be used to schedule MZ irrigation

Abstract

Irrigation scheduling decision-support tools can improve water use efficiency by matching irrigation recommendations to prevailing soil and crop conditions within a season. Yet, little research is available on how to support real-time precision irrigation that varies within-season in both time and space. We investigate the integration of remotely sensed vegetation index time-series, soil moisture sensor measurements, and root zone simulation forecasts for in-season delineation of dynamic management zones (MZ) and variable rate irrigation scheduling. In a 5.8-ha maize field in northeastern Spain, unsupervised classification of 2018 Sentinel 2 vegetation sensing time-series delineated dynamic MZs. The number and spatial extent of MZs changed through the growing season. A network of inexpensive soil moisture sensors was used to interpret spatiotemporal changes of Sentinel 2 data. Water content was a significant contributor to changes in crop vigor across MZs through the growing season. Real-time cluster validity function analysis provided in-season evaluation of the MZ design. For example, the total within-MZ daily soil moisture relative variance decreased from 85% (early vegetative stages) to below 25% (late reproductive stages). Finally, using the Hydrus-1D model, a workflow for in-season optimization of irrigation scheduling and water delivery management was tested. Data simulations indicated that crop transpiration could be optimized while reducing water applications between 11 and 28.5% across the dynamic MZs. The proposed integration of spatiotemporal crop and soil moisture data can be used to support management decisions to effectively control outputs of *crop* × *environment* × *management* interactions.

Keywords: Remote sensing; Spatial variability; Temporal variability; Precision agriculture; Soil moisture; Hydrus-1D

1. INTRODUCTION

Irrigated agriculture is essential to global food production, especially because of projected population growth (Döll, 2002). Irrigation water is commonly applied uniformly over an entire field. Yet, field soil water content is typically non-uniform because of spatial variability in soil hydraulic properties (Hawley, 1983), topography (Burt and Butcher, 1985), and vegetation growth (Le Roux et al., 1995). When field spatial variability is significant (Baveye and Laba, 2014; Thorp, 2019), modified water management that accounts for variability may improve the cost-effectiveness of irrigation (Liang et al., 2016; Martini et al., 2017) by increasing for instance water use efficiency and crop yields and decreasing nutrient leaching.

Precision agriculture seeks to optimize farming operations via site-specific management plans that vary the application of nutrients and water across a field based on variations in soil and crop conditions (Zhang et al., 2002). Management is prescribed over contiguous areas that have homogeneous soil properties and crop conditions. These areas are called management zones (MZ). Different clustering methods, including *k*-mean, ISODATA, and Gaussian Mixture, are available for delineating MZs based on different data sources (Schepers et al., 2004; Martinez-Casasnovas et al., 2012; Galambošová et al., 2014). Commonly, yield maps, topography, remote sensing data, and soil apparent electrical conductivity are used to delineate MZs (Liu et al., 2018; Scudiero et al., 2018; Ohana-levi et al., 2019). Remote sensing crop-canopy data is frequently used in agriculture because it is noninvasive and data can be downloaded without any cost (Fontanet et al., 2018).

Several researchers have defined MZs in specific fields with the goal of increasing crop yield and decreasing water use. Inman et al. (2008) and Schenatto et al. (2015) delineated MZs with NDVI data and different crop indices. Liu et al. (2018) delineated MZs based on yield and band vegetation indices maps. Scudiero et al. (2013) argued that spatial information on soil properties known to affect plant growth should guide MZ delineation. They modeled maize yield spatial variability as a function of salinity, texture, carbon content and bulk density, using geospatial apparent soil electrical conductivity and bare soil reflectance measurements as proxies for these soil properties. A similar study was presented by Reyes et al. (2019), in which MZs were defined with NDVI data and complemented with soil properties. Georgi et al. (2018) developed an algorithm to delineate MZs automatically based on remote sensing data. However, one of the disadvantages of this algorithm is that it does not work properly on fields with strong time-dependent spatial patterns. All the studies cited above consider MZs to be static and assume no dynamic pattern during the growing season. In fields where crop spatial patterns change over time, some researchers have advocated for MZ delineation to also be dynamic (Evans et al., 2013; Haghverdi et al., 2015; Cohen et al., 2016; Scudiero et al., 2018).

Water content sensors constitute a vital tool for real-time monitoring of water content dynamics in the field. Although sensors monitor water content at a single point, spatial and temporal variations of soil water content and their interactions with crops can be analyzed if several sensors are installed across the field (Biswas and Si, 2011; Biswas, 2014; Yang et al., 2016; Huang et al., 2019). These measurements can provide information about the source of variability between different MZs and aid in their delineation.

In this study, we integrate crop spatial and temporal information from high-resolution remote sensing, soil water sensor data, and numerical model simulations to investigate irrigation scheduling for dynamic management zones. Specifically, we: i.) characterize the spatial and temporal dynamics of crop-soil-water relations, ii.) delineate and evaluate temporally dynamic management zones for variable rate irrigation, and iii.) provide a workflow for in-season optimization of irrigation scheduling and water delivery management.

2. MATERIALS AND METHODS

2.1 Study Site

The research site was a 5.8-ha maize (*Zea mays* L.) field located in Raïmat, about 170 km west of Barcelona, Spain (Fig.1). The study region has a semi-arid climate. Summer temperatures average 24 ºC, with several days above 40 ºC. Summer is the dry season, with rainfall of 45 mm.

Land use at the study site has changed over the years (Fig. A.1 of Appendix A). Originally, the site was a forest where no tillage occurred. Approximately 30 years ago, the land was converted to a vineyard. The topography of the field was modified, with soil being added or removed in various sections, such that the site can now be regarded as having an anthropogenic soil. In 2017, one year before this study, grapevines were removed and maize was grown at the site.

2.2 Sowing and Irrigation

The field was sectioned into four plots that were each sowed with a different maize variety (Fig.1). The varieties were, from west to east: p0937 (DuPont Pioneer, Johnston, IA), d6980 (DEKALB Genetics Corporation, Dekalb, IL), p1524 (DuPont Pioneer), and d6780 (DEKALB). All plots were sown on May 3, 2018, with a sowing density of 90000 seeds·ha^{-1}. Data from the seed companies indicated that the varieties planted on the west and east edges of the field (p0937 and d6780, respectively) grow slightly faster than those planted down the center (d6980 and p1524), although all varieties were anticipated to reach full maturity 125-165 days after sowing. Plants started to emerge on May 12, 2018. The site was harvested on September 22, 2018.

The field was irrigated with a Solid Set sprinkler system (Nelson Irrigation Corporation, Walla Walla, WA) having 15 x 15 m spacing. Water was delivered over 18 irrigation zones at a rate of 6.5 L·m^{-2}·h^{-1}. Total applied water during the season was 679 mm. Irrigation was applied uniformly over the field with scheduling and depths determined using a crop coefficient approach (FAO56). For most of the site, irrigation ended 115 days after sowing. But, in two 0.3-ha sections located at the north-east end of the site, irrigation was halted 74 days after sowing due to soil waterlogging.

2.3 Soil, Environment, and Crop Measurements

Field data were collected between May and September 2018. Soil moisture, soil and crop parameters, environmental variables, and remote sensing NDVI data were measured. In May 2018, 33 capacitive EC-5 soil moisture sensors (METER Group, Pullman, WA, USA) with an accuracy of $\pm$ 0.03 $cm^3 \cdot cm^{-3}$ (Campbell and Devices, 1986) were installed at 11 locations named P1, P2, …, and P11 (Fig.1). The sensors were installed at 15, 35, and 50 cm depths. Water content data were registered every 30 minutes using an EM5b data logger (METER Group).

At each station, three disturbed soil samples were collected at 0-5, 5-35, and 30-60 cm depth for organic matter (OM) and soil texture analyses. The Walkley-Black method was used to measure OM (Nelson and Sommers, 1996), whereas soil particle size distribution was measured according to the gravimetric method (Gee and Bauder, 1986). Particles were categorized into the following size classes: clay (soil particle diameter, D < 0.002 mm), fine silt (0.002 < D < 0.02 mm), coarse silt (0.02 < D < 0.05 mm) and sand (0.05 < D < 2 mm). Undisturbed soil cores were also collected at the same locations and depths for measuring soil hydraulic properties. The soil water retention curve (SWRC) and unsaturated hydraulic conductivity curve (HCC) were determined using a combination of three laboratory devices: Hyprop, WP4c, and KSat (METER Group). The van Genuchten model (van Genuchten, 1980) was fit to the measured curves using the RETC software (van Genuchten MTh, Leij FJ, 1991) to estimate saturated water content (θ_s), residual water content (θ_r), saturated hydraulic conductivity (K_s), and the shape parameters α and

n. Principal component analysis (PCA) (Abdi and Williams, 2013; Martini et al., 2017) was used to investigate the relationships between soil texture, OM, bulk density, and hydraulic parameters. The PCA calculations were done with Statistica 12 (StatSoft Inc. Tulsa, OK, USA).

A weather station consisting of an ECRN-100 rain gauge (METER Group), a cup anemometer (Davis Instruments, Hayward, CA, USA), and PYR pyranometer and VP-4 relative humidity and temperature sensors (METER Group) was installed 150 m from the north-east corner of the field. The measured temperature, wind speed, relative humidity, and solar radiation were used to calculate daily reference evapotranspiration (ET_0) using the Penman-Monteith equation as specified in FAO Irrigation and Drainage Paper No. 56 (Allen et al, 1998; hereafter "FAO56"). The estimated ET_0 was converted into daily water requirements or potential evapotranspiration (ET_c) using the maize crop coefficient (k_c) from FAO56. Maximum and minimum daily temperature measurements were used to calculate growing degree days (GDD) according to FAO56 and to determinate reference maize growing stages (Ritchie et al., 1997).

Remote sensing data from Sentinel 2 were used to determine normalized difference vegetation index ($NDVI$) (Rouse et al., 1974),

$$NDVI = \frac{(NIR - Red)}{(NIR + Red)} \tag{1}$$

where NIR and Red are measured reflectance values in the near-infrared and visible red regions, respectively. $NDVI$ was used to evaluate spatial variability in the field. Remote sensing data were downloaded with 10-m spatial resolution every 5 days unless there was cloud coverage. The first and last images downloaded were the 15th and 135th day after sowing. Remote sensing data were processed with the Sentinel application platform (SNAP) software (Zuhlke et al., 2015).

2.4 Management Zones Delineation

Sentinel 2 NDVI was used to characterize the spatial variability of crop vigor through the season. A k-means (also known as "fuzzy c-means") unsupervised clustering algorithm (Odeh et al., 2010) was used to classify the NDVI data into temporally dynamic MZs. The Grouping Analysis tool in ArcMap 10.4.1 (ESRI, Rdlands, CA) was used for the MZ delineation. Anytime a new Sentinel 2 NDVI scene was available at the site, a new MZ scheme was delineated. Designs having 2 to 6 MZs were considered. The Calinski–Harabasz criterion (CHC) (Harabasz et al., 1974), Eq. (2), was used to evaluate the clusters and MZ delineations and select the optimum number of MZs. The CHC, also known as a pseudo F-statistic, measures the ratio of between-MZ differences and within-MZ similarity. It is formulated as:

$$\mathrm{CHC} = \frac{BMZSS/(MZn - 1)}{WMZSS/(N - MZn)} \tag{2}$$

where N is the number of pixels, MZn is the number of considered zones, $BMZSS$ is the between-zones sum of squares, and $WMZSS$ is the within-zone sum of squares. Large CHC values indicate high within-MZ homogeneity and between-MZ heterogeneity.

The $NDVI$ averages and maximum and minimum values within each MZ were calculated for further comparison between different MZs. MZs were not defined for the beginning of the season (0-20 day after sowing) because plants had not yet germinated or were not big enough to influence $NDVI$, and for the end of the season (beyond 130 days after sowing) because in that period the crop is in a late phenological stage and not irrigated. Differences in soil properties across MZs over time were assessed using a Kruskal-Wallis (Kruskal and Wallis, 1952) rank test (i.e., a non-parametric analysis of variance), calculated with Statistica 12.

Additionally, we considered an alternative static delineation scheme, subdividing the site into four contiguous fields corresponding to the planted maize varieties. The CHC was calculated for each available $NDVI$ scene to compare the variety-based MZ approach to the dynamic $NDVI$-based MZ delineation.

2.5 Management Zone Available Water

Soil-water status for the MZs was modeled as plant available water (AW) (Liang et al., 2016; Vellidis et al., 2016; Zurweller et al., 2019):

$$AW^{j}(t) = \frac{1}{Z_{\mathrm{T}}} \sum_{m} \left(\frac{\theta^{j,m}(t) - \theta_{\mathrm{wp}}^{j,m}}{\theta_{\mathrm{fc}}^{j,m} - \theta_{\mathrm{wp}}^{j,m}} \right) \Delta z^{m} \tag{3}$$

where $AW^{j}(t)$ is the profile average available water at monitoring station j and time t, m indexes the measurement depths, Δz^{m} (cm) is the depth increment associated with the moisture sensor at depth m, $Z_{\mathrm{T}} = \sum \Delta z_{m}$ (cm) is the total soil profile depth, $\theta^{j,m}$ ($\mathrm{cm^3 \cdot cm^{-3}}$) is soil water content, $\theta_{\mathrm{wp}}^{j,m}$ ($\mathrm{cm^3 \cdot cm^{-3}}$) is the wilting point (water content at -1500 kPa), and $\theta_{\mathrm{fc}}^{j,m}$ ($\mathrm{cm^3 \cdot cm^{-3}}$) is field capacity (determined using the method of Twarakavi et al., (2009)). The AW for a MZ was defined to be the average AW for all monitoring stations located within the MZ. Note that the MZ design changed over the growing season, so the MZ membership of some stations also changed. In addition to the CHC calculation on the $NDVI$ data, the spatiotemporal variability of AW was also used for in-season evaluation of the dynamic MZ-design. Following Fraisse et al., (2001), we calculated the daily weighted within-MZ AW variance (4),

$$S_{MZ_i}^{2} = \frac{N_{S_i} N_t}{N_S N_t} \times \frac{1}{N_{S_i} N_t} \sum_{j,k} \left[AW^{j}(t_k) - \overline{AW_i} \right]^{2} \tag{4}$$

where $S_{MZ_i}^{2}$ is the daily weighted AW variance within management zone *i*; j indexes the monitoring stations within management zone *i*; *k* indexes the measurement times during the current day; N_{S_i} is the number of stations in management zone *i*; $N_S (= 11)$ is the total number of stations in the field; $N_t(=48)$ is the number of measurements per day (every 30 min), AW^j is defined by (3), and $\overline{AW_i}$ is the average profile AW across monitoring stations in management zone i and measurement times in the current day. The total within-zone variance is equal to the sum of the weighted within-zone variances, $S^2 = \sum_i S^2_{MZ_i}$. By comparing S^2 with the total daily field-wide AW variance, it is possible to determine how much was gained in terms of AW uniformity by dividing the field into MZs (Fraisse et al., 2001).

3. RESULTS

3.1 Soil Properties

Texture, OM contents and bulk density (ρ_b) values measured at each station are reported in Table 1. The soil texture classes (USDA system) of samples taken from the 11 stations were clay loam (42.4 % of samples), loam (42.4%), and silty clay loam (15.2%). Stations on the east side (P1, P6, P7, P11) of the field had, on average, lower sand and higher silt and clay contents than those on the west. Average OM contents ranged between 0.57 and 1.96 %, which is typical for agricultural soils in the region (Romanyà and Rovira, 2011). Fitted and measured parameters for the soil hydraulic properties measured at each station are reported in Table 2. Consistent with the spatial trend in soil texture noted previously, the SWRCs measured on the east side of the study site (stations P1, P6, P7, P11) had lower fitted *n* values than in the rest of the site. On the wet end of a retention curve, a lower *n* value corresponds to a more gradual transition in water content as pressure head changes. Figure A.2 of Appendix A compares SWRCs observed at stations on the west (P9) and east (P11) sides of the field.

The principal component analysis (PCA) indicated that 8 principal components were needed to explain 95% of the variability in the soil dataset. The first three components, PC1 (30.9%), PC2

(18.6%), and PC3 (15.9%), explained around two thirds of the variance in the soil dataset. Particularly, PC1 indicated that clay content clustered (was positively correlated) with θ_{wp}, θ_{fc}, and α. The PC1 also indicated that clay content was negatively correlated with sand content, θ_r, and n. Further detail about PC1, PC2, and PC3 are reported in Fig. A.3 of Appendix A.

3.2 Remote Sensing and Dynamic Management Zones Delineation

The site average, minimum, and maximum $NDVI$ values for each available Sentinel 2 scene are reported in Fig. 2a. The changes in average $NDVI$ generally corresponded to the evolution of ET_c at the site, consistent with reports for maize grown in Mediterranean climates in other studies (Toureiro et al., 2017; Segovia-Cardozo et al., 2019). Figure 2b shows that cumulative input water (irrigation and precipitation) (618 mm) exceeded by 10.2% the site-wide cumulative ET_c (561 mm). At the bottom of Fig. 3, reference growing stages for maize at the site are shown (Ritchie et al., 1997). Varieties at the site took 120 to 130 days to reach maturity. Thus, we considered the reference growing stages to be representative for all maize varieties grown at the site. $NDVI$ and ET_c were low during the early vegetative stages, had maximum values during the late vegetative stage (VT) through the beginning of the reproductive stages (R1-R6), then decreased after R6. The temporal changes of $NDVI$ at the site are comparable to those observed in other studies on maize (Viña et al., 2004). In the early vegetative stages (V0 to V5), the $NDVI$ range of each Sentinel 2 scene was narrow. In later vegetative stages and early reproductive stages, the $NDVI$ ranges were much larger, indicating considerable variability in crop status (greenness, health) at the site.

Figure 3a shows the spatiotemporal changes of $NDVI$ at the sites. Areas with high and low $NDVI$ were observed at the site throughout the growing season. However, the $NDVI$ spatial patterns changed over time, suggesting that homogeneous or static site-specific management may be inadequate to address crop needs over time at this site. Figure 3b shows the dynamic MZ delineation obtained with unsupervised clustering of the $NDVI$ data. Through the growing season, the number of MZs, as well as their spatial distribution, changed. At the beginning of the season, until 50 days after sowing, the CHC indicated that three MZs were optimal for identifying homogeneous zones at the site. The MZ1 covered the north-west side of the site and had the highest $NDVI$ values; the MZ2 had intermediate $NDVI$ and spanned across the south of the site until the 45th day after sowing and after that over the south-west only. The MZ3 had lower $NDVI$ values and was initially the north-eastern side of the site, then covered the entire western side of the field at 45 days after sowing. From the 50th day after sowing, the CHC indicated that four clusters were best at identifying areas with homogeneous $NDVI$. MZ1 and MZ2 remained relatively similar to their early season delineations. The MZ4 identified an area of moderately low $NDVI$ at the south-eastern portion of the site, whereas MZ3, on the north-eastern side of the site, was characterized by the lowest $NDVI$ values. The spatial patterns of the four MZs changed only slightly over time, until the 130th day after sowing, when the size of MZ3 increased remarkably while MZ4 decreased. The unsupervised $NDVI$ clustering was compared to dividing the site into four blocks, one for each maize variety. Figure 3c shows the CHC values for $NDVI$ clustering into dynamic MZ and into varietal-based blocks through the growing season. The dynamic MZ-design strategy had larger CHC values for the entire growing season than the variety-block strategy, indicating that the dynamic MZs identified by unsupervised clustering had more homogeneous $NDVI$ than the varietal blocks.

Figure 3a shows contrasting $NDVI$ values between the eastern and western side of the field, especially visible along the boundary between the d6980 and p1524 varieties. The boundary between the d6980 and p1524 varieties seemed to be a big factor in the determination of the boundary between eastern (MZ1 and MZ2) and western (MZ3 and MZ4) zones from 55 to 120 days after sowing (Fig. 3b). Figure A.1.f of Appendix A shows the p1524 and d6780 varieties doing relatively poorly in July 2018. So, in addition to different soil hydraulic properties on the east side of the field, crop genetics (e.g., pest resistance, germination rate between the varieties) and uneven management (e.g., mechanical sowing, fertilization, soil tillage) could have been contributing factors to the poor performance of the p1524 and d6780 varieties. Changes in MZ delineation over time led to some changes in MZ membership for certain soil-water monitoring stations (Table 3). These changes occurred frequently in the early vegetative stages (until 54 days after sowing). No MZ membership change occurred in the late vegetative and reproductive stages. The MZs were characterized by contrasting soil properties throughout the season. The MZ had significantly ($p<0.05$) different PC1 scores throughout the season according to the Kruskal Wallis test: MZ1 and MZ2 were characterized by low PC1 scores, whereas MZ3 and MZ4 were characterized by the highest PC1 scores (Fig. A.3 of Appendix A).

3.3 NDVI and Applied Water

Changes in $NDVI$ and AW across MZs are depicted in Fig. 4a (MZ1), 4b (MZ2), 4c (MZ3), and 4d (MZ4). Through the growing season, $NDVI$ in MZ1 and MZ2 was higher than in MZ3 and MZ4. Furthermore, $NDVI$ was slightly higher in MZ1 than in MZ2. Average AW in MZ1 was close to 1 (i.e., water content was near θ_{fc}) throughout the entire growing season. Average AW in MZ2 was greater than 1 at the beginning of the season (until 45 days after sowing) and then very close to 1 through the end of the growing season. Portions of MZ3 and MZ4 had lower $NDVI$ values than MZ1 and MZ2. In these areas, irrigation was likely excessive. AW was considerably higher than 1 for the entire vegetative growth of maize and during the early reproductive stages.

Once irrigation was halted in the northeastern corner of the site (i.e., approximately over the area comprised by MZ3) at 74 day after sowing, the AW in MZ3 gradually decreased until the end of the season, while $NDVI$ in MZ3 remained stable. Halting irrigation in the northeastern corner of the site had little-to-no effect on the spatial extent of MZ3 and the other MZs, as shown in Fig. 3c. The analysis of the daily total within-MZ AW variance (S^2) provided further support for the use of $NDVI$ to identify areas with similar AW conditions at the site. In Fig. 4e, the calculated total MZ variance is normalized by the daily whole-site AW variance. Especially beyond 45 days after sowing (the beginning of the VT growth stage), the normalized within-MZ variance is much less than 1, showing that a large part of the total AW variance was explained by splitting the site into dynamic MZs delineated based on an analysis of $NDVI$. Fraisse et al. (2001) used yield within-zone variance to evaluate soil-derived MZs at the end of the season. Our results suggest that daily $AW\ S^2$ could also be used for in-season evaluation of management zone designs.

4. DISCUSSION

4.1 NDVI and irrigation scheduling simulations

The AW and $NDVI$ time series data show that soil water content was a major factor determining $NDVI$ spatiotemporal variability at the site. $NDVI$ is an indicator of maize crop health, and several studies have found positive correlations between $NDVI$, AW, and crop growth (Scudiero et al., 2014; West et al., 2018). However, those studies were for water scarce conditions. Crop stress and reductions in growth can occur from too much water in the soil profile as well as too little (Feddes et al., 1978). In the current study, where maize was grown under nearly waterlogged conditions for most of the growing season (Fig. 4), changes in $NDVI$ and AW between consecutive Sentinel 2 scenes were negatively correlated, with Pearson r equal to -0.64 (MZ1), -

0.87 (MZ2), -0.79 (MZ3), and -0.83 (MZ4) (all significant at $p<0.05$). Thus, as has been noted elsewhere (Shanahan et al., 2008; Long et al., 2015; Quebrajo et al., 2018; Scudiero et al., 2018), $NDVI$ data alone should not be used to make irrigation management decisions; $NDVI$ (and/or other plant canopy information) should be integrated with soil information to properly understand plant processes at a site.

With respect to within-season management decisions, one way to make a connection between $NDVI$-based dynamic management zone delineation and soil conditions would be to use a simulation model to make within-season forecasts of soil and crop conditions for different management options. In the remainder of this paper, we determine a hypothetical optimal irrigation schedule for each growing stage using the simulation/optimization approach developed by Fontanet et al. (Vadose Zone Journal, submitted). We first show that a physically based simulation model, Hydrus-1D (Šimůnek et al., 2016), is consistent with NDVI-based zoning by simulating the field experiment and demonstrating agreement between measured AW and simulated available water (SAW), as well as showing a correspondence between simulated transpiration (ST_a) rates and $NDVI$. Next, we use the calibrated model to investigate what-if irrigation scenarios, calculating a hypothetical irrigation scheduling table for each dynamic MZ that could have been generated from NDVI within season to guide irrigation.

4.2 Hydrus-1D Available Water and Transpiration Simulations

The well-known Hydrus-1D model solves the Richards Equation numerically to simulate variably saturated water flow and root water uptake in soils. The model inputs and parameterizations used in our simulations are detailed in Appendix B. Simulations of the experiment for differing monitoring locations all used the same inputs and parameters except for (i.) the soil hydraulic properties, which were measured at each station during the field campaign (Table 2), and (ii.) the irrigation boundary condition, which differed only for stations P10 and P11 because irrigation was stopped during the experiment.

In Fig. 5, daily observed AW for each station is compared with daily-simulated available water (SAW). Generally, good agreement between AW and SAW existed for all stations, although it is acknowledged that the AW time courses were relatively non-dynamic. Still, the simulations were done using independently measured hydraulic properties and without any parameter fitting, so the agreement is quite good (modeling details can be found in Appendix B). Missing data towards the end of the season in P7 was due to rodents chewing on the sensor cables.

Figure 6 shows the weekly-simulated actual transpiration (ST_a) at each MZ and the potential transpiration (T_p) at the site. At MZ1 and MZ2, ST_a weekly averages were always equal or near the potential transpiration. At MZ3 and MZ4, ST_a weekly values were remarkably lower than the potential. There was good correspondence between ST_a and $NDVI$ at each MZ, with a Pearson *r* of 0.6 (MZ1), 0.51 (MZ2), 0.69 (MZ3), and 0.82 (MZ4). In agreement with the results discussed for $NDVI$ and AW data (section *3.2. Remote Sensing and Dynamic Management Zones Delineation*), low ST_a values at MZ3 and MZ4 were due to waterlogging (root water uptake and transpiration is reduced in the model whenever simulated soil water content exceeds a threshold value; see Appendix B). Stations in MZ3 and MZ4 (see Table 3) had AW and SAW over 1 for most of the growing season (Fig. 4).

4.3 Irrigation scheduling for within-season decision making

We adopted the method of Fontanet et al. (Vadose Zone Journal, submitted) to investigate optimal irrigation scheduling for dynamic MZs. In this method, irrigation of duration τ [T] is prescribed whenever the soil moisture content decreases below a critical level (h^*) as indicated by readings from a soil water pressure head sensor(s). The irrigation rate is assumed to be a fixed constant for a given irrigation system. The recommended duration and threshold are determined using a simulation/optimization procedure. Simulations are made using forecasted daily or weekly crop water demand (reference ET_0) and a range of values for the irrigation scheduling parameters, h^* and τ. The optimal parameter values are those that maximize seasonal transpiration in the simulations (transpiration being, for many agronomically important crops, proportional to marketable yield). In adapting the simulation/optimization method, we make separate recommendations for each MZ, and update them whenever there is a change in MZ station membership. The recommended values of h^* and τ for a given MZ are the average values determined for monitoring stations within the zone. For simplicity, we use in this example the known daily potential ET_0 for the forecasted model boundary condition (rather than historical data which would be necessary for actual within-season forecasts). Also, as the season progressed, we triggered irrigation based on readings from progressively deeper sensors. In principle, when multiple sensor depths are available, the sensor depth could be treated as an additional optimization parameter. Full details on our implementation of the Fontanet et al. (Vadose Zone Journal, submitted) procedure are given in Appendix C.

Although the Fontanet et al. (Vadose Zone Journal, submitted) method prescribes an optimized irrigation schedule, in practice a grower may not be able to irrigate exactly according to a schedule and sensor readings, particularly when there are multiple management zones. Therefore, we also calculated recommended irrigation durations (or, equivalently, irrigation amounts) for soils that have become dryer than the “optimal” irrigation trigger point.

The resulting irrigation scheduling calendar for dynamic-MZ irrigation is presented in Table 4. Optimal irrigation strategies for each growth stage are shown in bold. The other table entries show irrigation recommendations for field sections that are dryer than the optimal trigger point. Strategies alternatives in order to allow agriculture to readjust irrigation in case that some parts of the field do not follow the optimal irrigation recommendation. As a general term, and following the tendency of this work, there are two main optimal parameter groups for irrigation scheduling; (i) MZ1 with τ=[1.9, 2.6] h·d^{-1} and h^*=[-23.3, -30] kPa; MZ2 with τ=[1.9, 2.0] h·d^{-1} and h^*=[-18.3, -30] kPa. Here, the intervals reflect the temporal variations of optimal values associated with the different growing stages. These parameters represent medium frequent and short irrigations. (ii) MZ3 with τ=2 h·d^{-1} and h^*=[-10, -20] kPa; MZ4 with τ=[2.0, 2.3] h·d^{-1} and h^*=[-10, -16.7] kPa. They represent very frequent and short irrigations. The other situation that can be in the site is when the pressure head threshold is smaller than the corresponding optimal value. In this case, τ increases because water consumed might be supplied until to arrive similar values of simulated actual transpiration as the optimal irrigation scheduling.

Table 5 compares seasonal transpiration and irrigation simulated with optimal scheduling versus the amounts obtained simulating the field experiment. For MZ1 and MZ2, the optimal schedule recommended 11 to 13 % less water and increased transpiration by 5 to 8 %. For MZ3, 29 % less water was recommended, with an increase in transpiration of 24 %. And for MZ4, a 17 % reduction in irrigation corresponded to a massive 53% increase in transpiration. These results are consistent with our earlier findings and discussion indicating the field was over-irrigated, especially in MZ3 and MZ4.

6. CONCLUSIONS

Irrigation scheduling is complicated by the spatial and temporal variability of a number of variables and parameters. In this work, we investigated a workflow for improved precision irrigation scheduling using data from a maize field where four maize varieties were sown. The workflow is based on dynamic MZ delineation with unsupervised $NDVI$ clustering. We found that MZs based on NDVI clustering were better able to statistically represent field variability than MZs based on maize variety. Additionally, the optimal number and spatial configuration of the MZs were found to change over the growing season. The highest number of MZs was 4. Management Zones 1 and 2 (MZ1 and MZ2) corresponded to field sections where NDVI values reflected a typical maize crop performance, whereas MZ3 and MZ4 featured relatively low $NDVI$ values indicative of poor maize growth.

Soil water content data were analyzed to show that the variation in crop performance was attributable to soil hydraulic properties, soil available water, and over-irrigation. Further, a relationship existed between NDVI and soil available water. The results indicated that soil available water could potentially also be used for, or incorporated into, in-season evaluation of management zone designs.

Lastly, we proposed a method of combining dynamic management zone delineation with Hydrus 1-D model forecasts for irrigation scheduling. The field experiment was first simulated to confirm the model parameterization and demonstrate its consistency with the obtained NDVI and soil water content data. We then used model simulations to determine an optimal zonation and irrigation calendar for different crop growth stages that could have been generated and updated in real time during the season. Simulations with the optimized irrigation schedule produced an increase in transpiration and a decrease in water use as compared to the field trial (which, again, was over-irrigated). The improvement was especially remarkable for MZ3 and MZ4, where irrigation was reduced by 28.5 and 16.6 %, and transpiration increased by 23.9 and 52.6 %, respectively.

In summary, we note that although NDVI is useful for dynamically delineating management zones, for irrigation scheduling, it is recommended that NDVI be combined with some additional measure of soil conditions. Low NDVI values may be indicative of poor crop performance, but without other information it is not possible to determine the cause nor recommend a remedial irrigation or management practice.

Appendix A. Supplementary figures

Supplementary material related to this article can be found, in the online version, at doi: #

Appendix B. Hydurs-1D Simulations

Hydrus-1D (Šimůnek et al., 2008, 2016) was used to simulated soil moisture dynamics and water balance components at each monitoring station. Each simulation spanned 105 days, from the 18th to the 123rd day after sowing. The 60 cm soil profile consisted of three layers/materials, as specified in Table 2. Soil hydraulic properties were specified using the van Genuchten-Mualem model (van Genuchten, 1980) as follows:

$$\theta(h) = \begin{cases} \theta_r + \dfrac{\theta_s - \theta_r}{(1 + |\alpha h|^n)^m} & h < 0 \\ \theta_s & h \geq 0 \end{cases} \tag{B.1}$$

and

$$K(h) = K_s S_e^{1/2} \left[1 - \left(1 - S_e^{1/m}\right)^m\right]^2, \tag{B.2}$$

where θ ($cm^3 \cdot cm^{-3}$) is the volumetric water content; h is the soil water pressure head (cm); θ_s ($cm^3 \cdot cm^{-3}$) is saturated water content; θ_r ($cm^3 \cdot cm^{-3}$) is residual water content; K_s ($cm \cdot d^{-1}$) is saturated hydraulic conductivity; n and α are shape parameters; $S_e = \frac{\theta-\theta_r}{\theta_s-\theta_r}$; and $m = 1 - 1/n$.

In Hydrus, root water uptake is simulated using a sink term S which has three parts, the potential transpiration rate (T_p) (cm·d^{-1}), the root density distribution (β) (cm^{-1}), and the dimensionless water stress function ($\alpha(h)$):

$$S(h,z,t) = \alpha(h,z,t)\beta(z,t)T_p(t) \qquad \text{(B.3)}$$

The actual transpiration rate (T_a) (cm·d^{-1}) is calculated by integrating Eq. (B.3) over the root zone L_R:

$$T_a = \int_{L_R} S(h,z,t)dz = T_p \int_{L_R} \alpha(h,z,t)\beta(z,t)dz \qquad \text{(B.4)}$$

Root depth was measured twice a month during the field campaign at one location. This information was used to parameterize the Hydrus root growth module.

Water stress ($\alpha(h)$) was modeled using the Feddes et al. (1978) function:

$$\alpha(h) = \begin{cases} \dfrac{h-h_4}{h_3-h_4} & h_3 > h > h_4 \\ 1 & h_2 \geq h \geq h_3 \\ \dfrac{h-h_1}{h_2-h_1} & h_1 > h > h_2 \\ 0 & h \leq h_4 \; or \; h \geq h_1 \end{cases} \qquad \text{(B.5)}$$

Parameterized by four critical values of pressure head, Eq. (B.5) defines maximal uptake ($\alpha = 1$) when the soil water pressure head is $h_2 \geq h \geq h_3$. Water uptake decreases linearly above or below that range ($h_3 > h > h_4$ or $h_1 > h > h_2$). And uptake is zero when $h \leq h_4$ or $h \geq h_1$. According to the Hydrus-1D database, the parameter values for maize are h_1 = -1.5, h_2 = -3.0, h_3 = -60. and h_4 = -800. kPa, respectively. The value of h_3 was allowed to vary as a function of evaporative demand as modeled by Hyrdurs-1D.

Three observation nodes were inserted in the domain at the same depths as the soil moisture sensors, 15, 35 and 50 cm. Soil moisture values simulated at the observation nodes were used to determine the simulated available water (SAW), using the same procedure as with the field data. The potential evaporation and transpiration rates were calculated by partitioning ET_c into potential evaporation (E_p) and transpiration (T_p) based on the canopy cover fraction (α) according to Raes et al. (2010). An atmospheric boundary condition was imposed at the surface and a free drainage condition was used at the bottom. Simulated actual transpiration (ST_a) and simulated applied irrigation (SAI) results from each station were extracted. ST_a and SAI were calculated by averaging stations located with the dynamic MZs.

Appendix C. Irrigation Scheduling

Irrigation scheduling was optimized using the methodology developed by Fontanet et al. (submitted). All soil, environmental and crop inputs are the same as described previously for the Hydrus-1D simulations (Appendix B). Possible values for the irrigation scheduling parameters were constrained to be $h^* \in$ {-10, -20, …, -100 kPa} and $\tau \in$ {1, 2, 3, 4 $h \cdot d^{-1}$}. The irrigation rate was constant (6.5 $L \cdot h^{-1} \cdot m^{-2}$). The soil depth used to trigger irrigation (Z_{tr}) changed during the growing season, becoming deeper as the season progressed. Irrigation parameters have been defined at each station and at different crop growing stages (V0-V5, V6-V10, V11-V15, VT, R1-R6). The optimal irrigation at each grow stage and MZ are the average values obtained for the stations located in the MZ.

Bibliography

Abdi, H., and L.J. Williams. 2013. Principal components analysis. Methods Mol. Biol. 930: 527–547. doi: 10.1007/978-1-62703-059-5_22.

Baveye, P.C., and M. Laba. 2014. Moving away from the geostatistical lamppost: Why, where, and how does the spatial heterogeneity of soils matter? Ecol. Modell. doi: 10.1016/j.ecolmodel.2014.03.018.

Biswas, A. 2014. Landscape characteristics influence the spatial pattern of soil water storage: Similarity over times and at depths. Catena 116: 68–77. doi: 10.1016/j.catena.2013.12.004.

Biswas, A., and B.C. Si. 2011. Application of continuous wavelet transform in examining soil spatial variation: A review. Math. Geosci. 43(3): 379–396. doi: 10.1007/s11004-011-9318-9.

Burt, T.P., and D.P. Butcher. 1985. Topographic controls of soil moisture distributions. J. Soil Sci. 36(3): 469–486. doi: 10.1111/j.1365-2389.1985.tb00351.x.

Campbell, C.S., and D. Devices. 1986. Calibrating ECH 2 O Soil Moisture Probes. : 2–4.

Cohen, Y., V. Alchanatis, Y. Saranga, O. Rosenberg, E. Sela, et al. 2016. Mapping water status based on aerial thermal imagery : comparison of methodologies for upscaling from a single leaf to commercial fields. Precis. Agric. doi: 10.1007/s11119-016-9484-3.

Döll, P. 2002. Impact of climate change and variability on irrigation requirements: a global prespective. Clim. Change 54: 269–293. papers2://publication/uuid/A172B730-6A69-45C8-8D12-88869ED1E5B8.

Evans, R.G., J. LaRue, K.C. Stone, and B.A. King. 2013. Adoption of site-specific variable rate sprinkler irrigation systems. Irrig. Sci. 31(4): 871–887. doi: 10.1007/s00271-012-0365-x.

Feddes, R.A., P.J. Kowalik, and H. Zaradny. 1978. Simulation of Field Water Use and Crop

Yield. Simulation Monograph. : 308. http://library.wur.nl/WebQuery/wurpubs/407104.

Fontanet, M., D. Fernàndez-garcia, and F. Ferrer. 2018. The value of satellite remote sensing soil moisture data and the DISPATCH algorithm in irrigation fields. Hydrol. Earth Syst. Sci. 22(11): 5889–5900.

Fraisse, C.W., K.A. Sudduth, and N.R. Kitchen. 2001. Delineation of Site-Specific management Zones by Unsupervised Classification of Topographic Atributes and Soil Electrical Conductivity. Am. Soc. Agric. Eng. 155 44(1): 155–166. doi: 10.1117/12.840574.

Galambošová, J., V. Rataj, R. Prokeinová, and J. Prešinská. 2014. Determining the management zones with hierarchic and non-hierarchic clustering methods. 60(2000).

van Genuchten MTh, Leij FJ, Y.S. 1991. The RETC code for quantifying the hydraulic functions of unsaturated soils. US Environ. Prot. Agency R. S. Kerr Environ. Res. Lab. Off. Res. Dev. Ada, OK.

van Genuchten, M.T. 1980. A Closed-form Equation for Prediccting Hydraulic Conductivity of Unsaturated Soils. Soil Sci. Soc. Am. J. 44(5): 892–898. doi: doi:10.2136/sssaj1980.03615995004400050002x.

Georgi, C., D. Spengler, S. Itzerott, and B. Kleinschmit. 2018. Automatic delineation algorithm for site-specific management zones based on satellite remote sensing data. Precis. Agric. 19(4): 684–707. doi: 10.1007/s11119-017-9549-y.

Haghverdi, A., B.G. Leib, R.A. Washington-Allen, P.D. Ayers, and M.J. Buschermohle. 2015. Perspectives on delineating management zones for variable rate irrigation. Comput. Electron. Agric. 117: 154–167. doi: 10.1016/j.compag.2015.06.019.

Harabasz, J., P. Scroll, and D. For. 1974. Communications in Statistics A dendrite method for cluster analysis. Commun. Stat. 1(3): 37–41. doi: 10.1080/03610927408827101.

Hawley. 1983. Journal of Hydrology, 62 (1983) 179--200. J. Hydrol. 62: 179–200. doi: 10.1016/0022-1694(83)90102-6.

Huang, J., A.E. Hartemink, F. Arriaga, and N.W. Chaney. 2019. Unraveling location-specific and time-dependent interactions between soil water content and environmental factors in cropped sandy soils using Sentinel-1 and moisture probes. J. Hydrol. 575(May): 780–793. doi: 10.1016/j.jhydrol.2019.05.075.

Inman, D., R. Khosla, R. Reich, and D.G. Westfall. 2008. Normalized difference vegetation index and soil color-based management zones in irrigated maize. Agron. J. 100(1): 60–66. doi: 10.2134/agronj2007.0020.

Kruskal, W.H., and W.A. Wallis. 1952. Use of Ranks in One-Criterion Variance Analysis Author (s): William H . Kruskal and W . Allen Wallis Published by : Taylor & Francis , Ltd . on behalf of the American Statistical Association Stable URL : http://www.jstor.org/stable/2280779 Accessed : 02. M J. Am. Stat. Assoc. 47: 583–621. doi: 10.1002/med.

Liang, X., V. Liakos, O. Wendroth, and G. Vellidis. 2016. Scheduling irrigation using an approach based on the van Genuchten model. Agric. Water Manag. 176: 170–179. doi: 10.1016/j.agwat.2016.05.030.

Liu, H., M.L. Whiting, S.L. Ustin, P.J. Zarco-Tejada, T. Huffman, et al. 2018. Maximizing the relationship of yield to site-specific management zones with object-oriented segmentation of hyperspectral images. Precis. Agric. 19(2): 348–364. doi: 10.1007/s11119-017-9521-x.

Long, D.S., J.D. Whitmus, R.E. Engel, and G.W. Brester. 2015. Net returns from terrain-based variable-rate nitrogen management on dryland spring wheat in Northern Montana. Agron. J. 107(3): 1055–1067. doi: 10.2134/agronj14.0331.

Martinez-Casasnovas, J.A., J. Agelet-Fernandez, J. Arno, and M.C. Ramos. 2012. Analysis of vineyard differential management zones and relation to vine development , grape maturity and quality. Spanish J. Agric. Res. 10(2): 326–337.

Martini, E., U. Wollschläger, A. Musolff, U. Werban, and S. Zacharias. 2017. Principal component analysis of the spatiotemporal pattern of soil moisture and apparent electrical conductivity. Vadose Zo. J. 16(10). doi: 10.2136/vzj2016.12.0129.

Odeh, I.O.A., A.B. McBratney, and D.J. Chittleborough. 2010. Soil Pattern Recognition with Fuzzy-c-means: Application to Classification and Soil-Landform Interrelationships. Soil Sci. Soc. Am. J. 56(2): NP. doi: 10.2136/sssaj1992.03615995005600020050x.

Ohana-levi, N., I. Bahat, A. Peeters, A. Shtein, Y. Netzer, et al. 2019. Original papers A weighted multivariate spatial clustering model to determine irrigation management zones. 162(February): 719–731. doi: 10.1016/j.compag.2019.05.012.

Quebrajo, L., M. Perez-Ruiz, L. Pérez-Urrestarazu, G. Martínez, and G. Egea. 2018. Linking thermal imaging and soil remote sensing to enhance irrigation management of sugar beet. Biosyst. Eng. 165: 77–87. doi: 10.1016/j.biosystemseng.2017.08.013.

Reyes, J., O. Wendroth, C. Matocha, and J. Zhu. 2019. Delineating Site-Specific Management Zones and Evaluating Soil Water Temporal Dynamics in a Farmer's Field in Kentucky. Vadose Zo. J. 18(1): 0. doi: 10.2136/vzj2018.07.0143.

Ritchie, S.W., J.J. Hanway, and G.O. Benson. 1997. How a corn plant develops.; Spec. Publ. 48.

Romanyà, J., and P. Rovira. 2011. An appraisal of soil organic C content in Mediterranean agricultural soils. Soil Use Manag. 27(3): 321–332. doi: 10.1111/j.1475-2743.2011.00346.x.

Rouse, R.W.H., J.A.W. Haas, and D.W. Deering. 1974. Monitoring Vegetation Systems in the

Great Plains with ERTS. Third Earth Resour. Technol. Satell. Symp. Vol. I Tech. Present. NASA SP-351: 309–317. https://ntrs.nasa.gov/search.jsp?R=19740022614.

Le Roux, X., T. Bariac, and a Mariotti. 1995. Spatial partitioning of the soil water resoucre between grasses and shrub compnents in a west African humid savanna. Oecologia 104: 145–155. doi: 10.1007/BF00328579.

Schenatto, K., E.G. Souza, C.L. Bazzi, and H.M. Beneduzzi. 2015. Management Zones with NDVI Data through Corn and Soybean Yield. First Conf. Prox. Sens. Support. Precis. Agric. (September). doi: 10.3997/2214-4609.201413856.

Schepers, A.R., J.F. Shanahan, M.A. Liebig, J.S. Schepers, S.H. Johnson, et al. 2004. Appropriateness of Management Zones for Characterizing Spatial Variability of Soil Properties and Irrigated Corn Yields across Years. Agron. J. 96(1): 195–203.

Scudiero, E., P. Teatini, D.L. Corwin, N. Dal Ferro, G. Simonetti, et al. 2014. Spatiotemporal response of maize yield to edaphic and meteorological conditions in a saline farmland. Agron. J. 106(6): 2163–2174. doi: 10.2134/agronj14.0102.

Scudiero, E., P. Teatini, D.L. Corwin, R. Deiana, A. Berti, et al. 2013. Delineation of site-specific management units in a saline region at the Venice Lagoon margin, Italy, using soil reflectance and apparent electrical conductivity. Comput. Electron. Agric. 99: 54–64. doi: 10.1016/j.compag.2013.08.023.

Scudiero, E., P. Teatini, G. Manoli, F. Braga, T. Skaggs, et al. 2018. Workflow to Establish Time-Specific Zones in Precision Agriculture by Spatiotemporal Integration of Plant and Soil Sensing Data. Agronomy 8(11): 253. doi: 10.3390/agronomy8110253.

Segovia-Cardozo, D.A., L. Rodríguez-Sinobas, and S. Zubelzu. 2019. Water use efficiency of corn among the irrigation districts across the Duero river basin (Spain): Estimation of local crop coefficients by satellite images. Agric. Water Manag. 212(February 2018): 241–251. doi: 10.1016/j.agwat.2018.08.042.

Shanahan, J.F., N.R. Kitchen, W.R. Raun, and J.S. Schepers. 2008. Responsive in-season nitrogen management for cereals. Comput. Electron. Agric. 61(1): 51–62. doi: 10.1016/j.compag.2007.06.006.

Šimůnek, J., M.T. van Genuchten, and M. Šejna. 2008. Development and Applications of the HYDRUS and STANMOD Software Packages and Related Codes. Vadose Zo. J. 7(2): 587. doi: 10.2136/vzj2007.0077.

Šimůnek, J., M.T. van Genuchten, and M. Šejna. 2016. Recent Developments and Applications of the HYDRUS Computer Software Packages. Vadose Zo. J. 15(7): 0. doi: 10.2136/vzj2016.04.0033.

Thorp, K.R. 2019. Long - term simulations of site - specific irrigation management for Arizona cotton production. Irrig. Sci. (0123456789). doi: 10.1007/s00271-019-00650-6.

Toureiro, C., R. Serralheiro, S. Shahidian, and A. Sousa. 2017. Irrigation management with remote sensing: Evaluating irrigation requirement for maize under Mediterranean climate condition. Agric. Water Manag. 184: 211–220. doi: 10.1016/j.agwat.2016.02.010.

Twarakavi, N.K.C., M. Sakai, and J. Šimůnek. 2009. An objective analysis of the dynamic nature of field capacity. Water Resour. Res. 45(10): 1–9. doi: 10.1029/2009WR007944.

Vellidis, G., V. Liakos, C. Perry, W.M. Porter, and M.A. Tucker. 2016. Irrigation Scheduling for Cotton Using Soil Moisture Sensors, Smartphone Apps, and Traditional Methods. : 772–780. http://vellidis.org/wp-content/uploads/2016/07/Vellidis-Beltwide-Paper-16779-Irrigation-Scheduling.pdf.

Viña, A., D.C. Gitelson, G. Rundquist, B. Keydan, Leavitt, et al. 2004. Monitoring Maize (Zea mays L.) Phenology with Remote Sensing. Agron. J. 96: 1139–1147. doi: 10.1007/978-1-4614-3103-9.

West, H., N. Quinn, M. Horswell, and P. White. 2018. Assessing vegetation response to soil moisture fluctuation under extreme drought using sentinel-2. Water (Switzerland) 10(7): 1–22. doi: 10.3390/w10070838.

Yang, Y., O. Wendroth, and R.J. Walton. 2016. Temporal Dynamics and Stability of Spatial Soil Matric Potential in Two Land Use Systems. Vadose Zo. J. 15(8): 0. doi: 10.2136/vzj2015.12.0157.

Zhang, N., M. Wang, and N. Wang. 2002. Precision agriculture*a worldwide overview Naiqian. Comput. Electron. Agric. 36: 113–132. doi: 10.1111/j.1751-1097.1990.tb01731.x.

Zurweller, B.A., D.L. Rowland, M.J. Mulvaney, B.L. Tillman, K. Migliaccio, et al. 2019. Optimizing cotton irrigation and nitrogen management using a soil water balance model and in-season nitrogen applications. Agric. Water Manag. 216(July 2018): 306–314. doi: 10.1016/j.agwat.2019.01.011.

Zuhlke M., Fomferra N., Brockmann C., Peters M., Veci L., Malik J., Regner P. SNAP (Sentinel Application Platform) and the ESA Sentinel 3 Toolbox; Proceedings of the Sentinel-3 for Science Workshop; Venice, Italy. 2–5 June 2015; p. 21.

Figures:

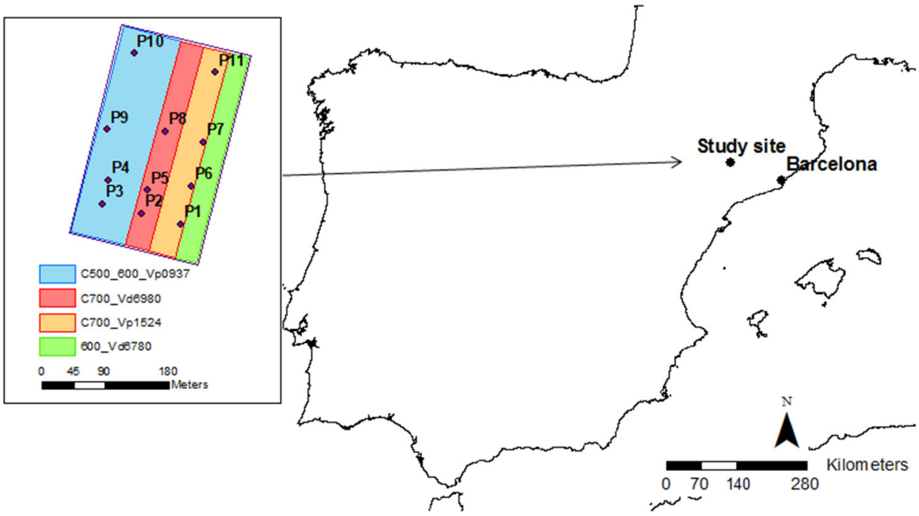

Figure 1. Study site location, soil moisture station locations, and maize variety plantings. The blue area represents maize variety p0937 (a combination of 500 and 600 series), the red area is variety d6980 (700 series), the yellow area is p1524 (700 series), and the green area is d6780 (600 series).

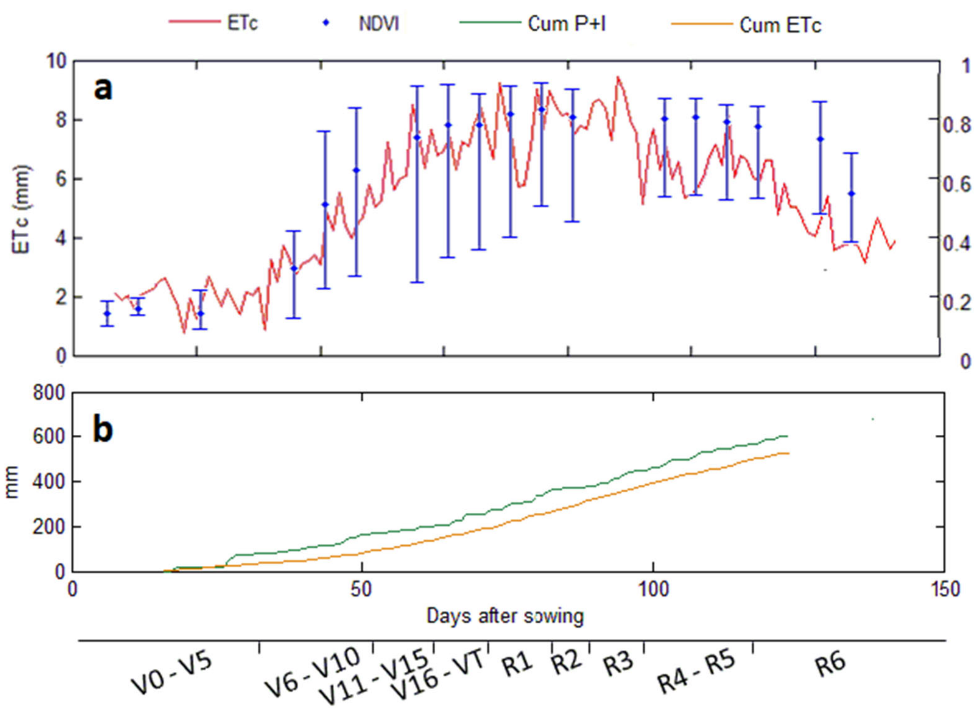

Figure 2. Field average evapotranspiration, NDVI, and cumulative water fluxes as a function of time and maize growth stage. The bars on the NDVI data indicate field maximum and minimum values. (V is vegetative stage; R is reproductive stage NDVI is Normalized Difference Vegetation Index; ETc is daily water requirements; Cum P+I is cumulative Precipitation and Irrigation; and Cum ETc is cumulative water requirements).

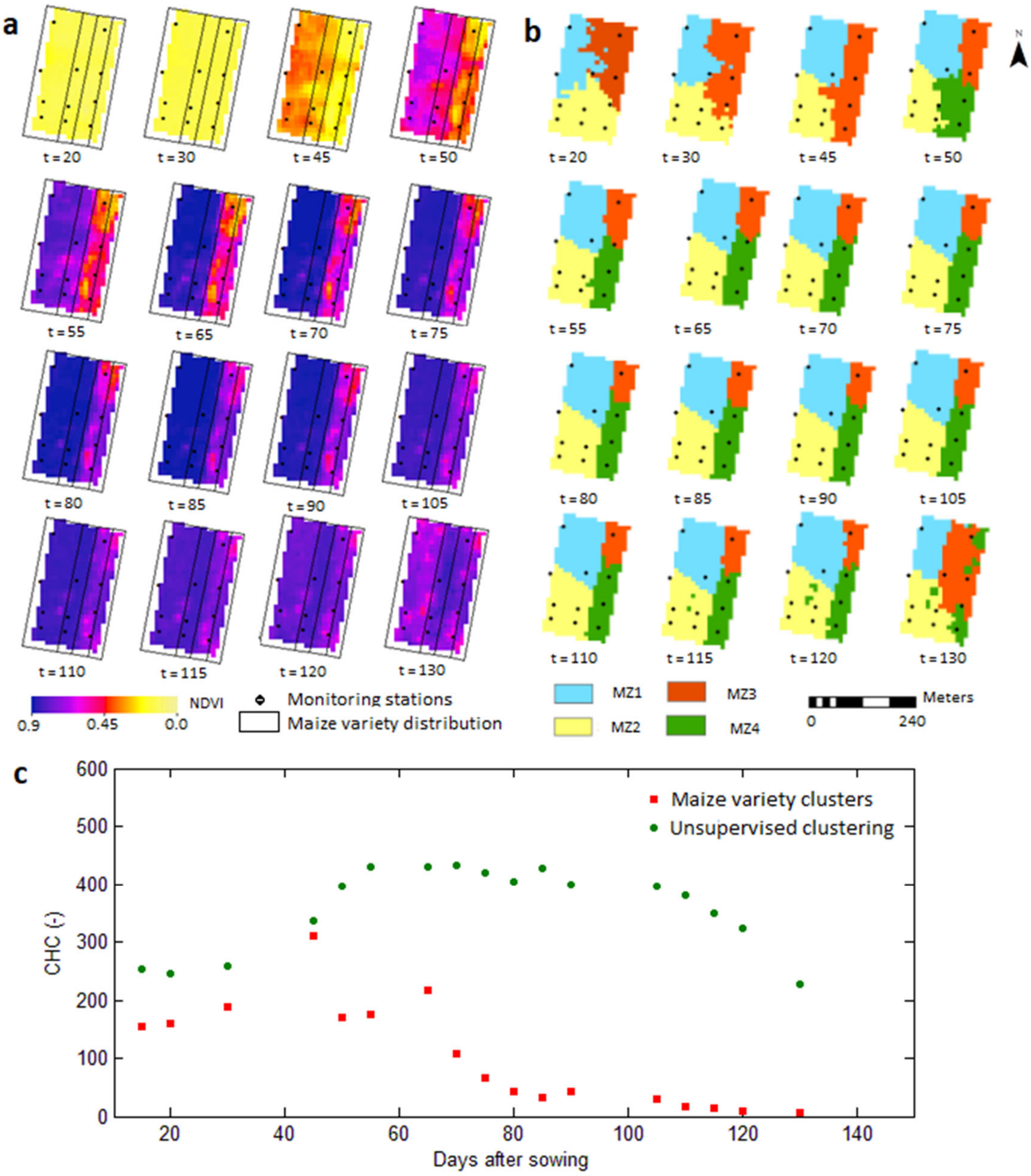

Figure 3. a) Normalized Difference Vegetation Index (NDVI) datasets measured by Sentinel 2 satellite through the growing season; b) dynamic management zone (MZ) delineation. The letter t indicates days after sowing; and c) Calinski-Harabaz criterion (CHC) for the NDVI grouped by maize variety (red squares) and with the unsupervised fuzzy-k clustering (green dots).

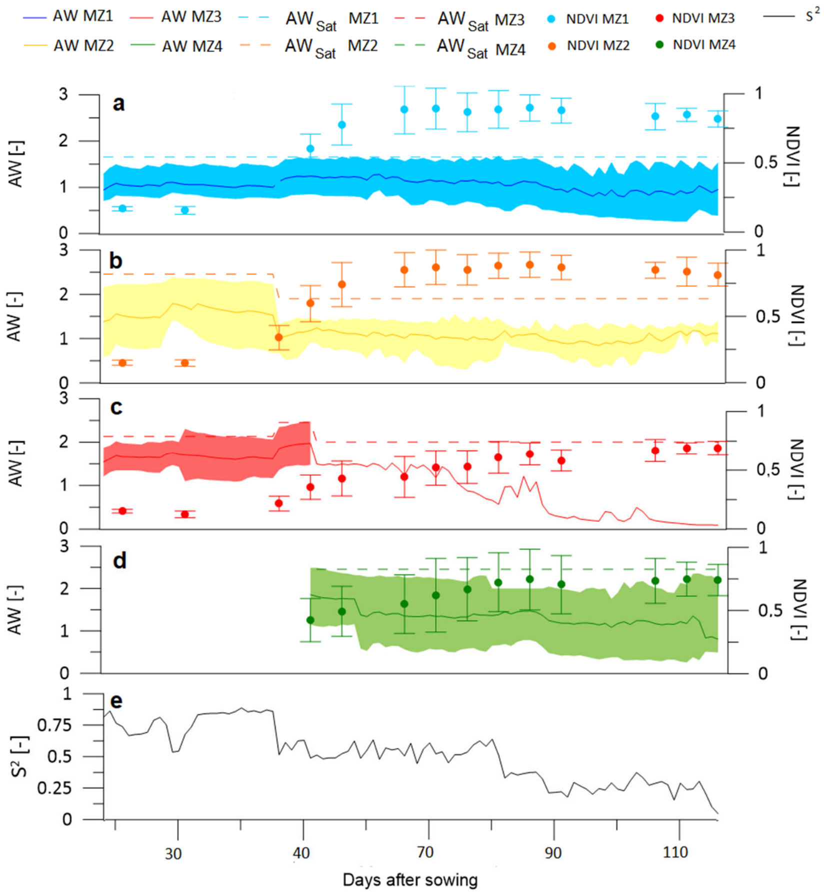

Figure 4. Soil profile available water (AW) and NDVI averages for a) MZ1, b) MZ2, c) MZ3, d) MZ4. Shaded areas represent the maximum in minimum AW at each MZ, while dash lines show available water saturated (AW_{sat}) (θ) and field capacity point (θ_{fc}). Error bars represents the maximum and minimum NDVI at each MZ. Note that AW = 1 corresponds to a soil water content equal to field capacity. Panel e) shows the daily total within-MZ weighted variance (S^2) of AW relative to the daily field-wide AW variance (i.e., S^2=1).

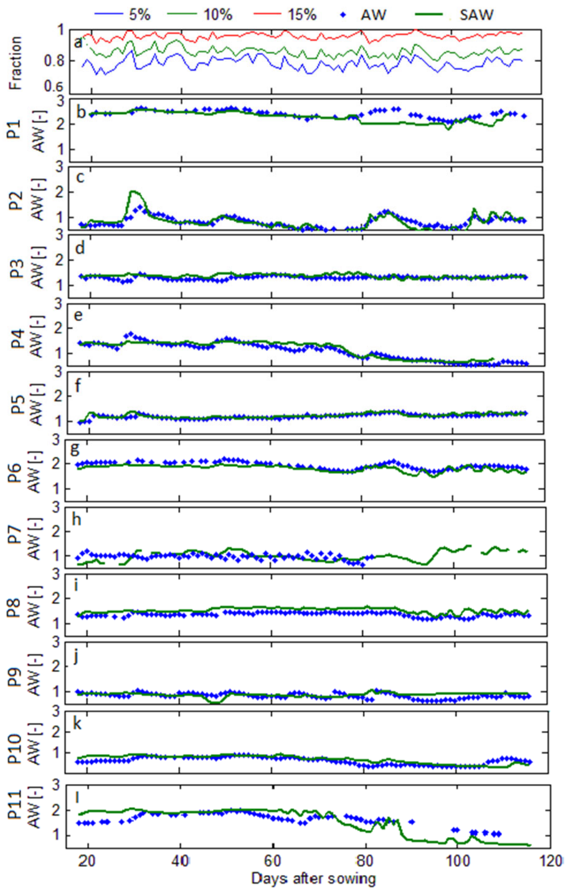

Figure 5. a) Evaluation of profile available water (AW) simulations showings the fraction of error greater than 5, 10, and 15%. b to l) Comparison between measured available water (AW) and simulated available water (SAW) at each station (P1 - P11).

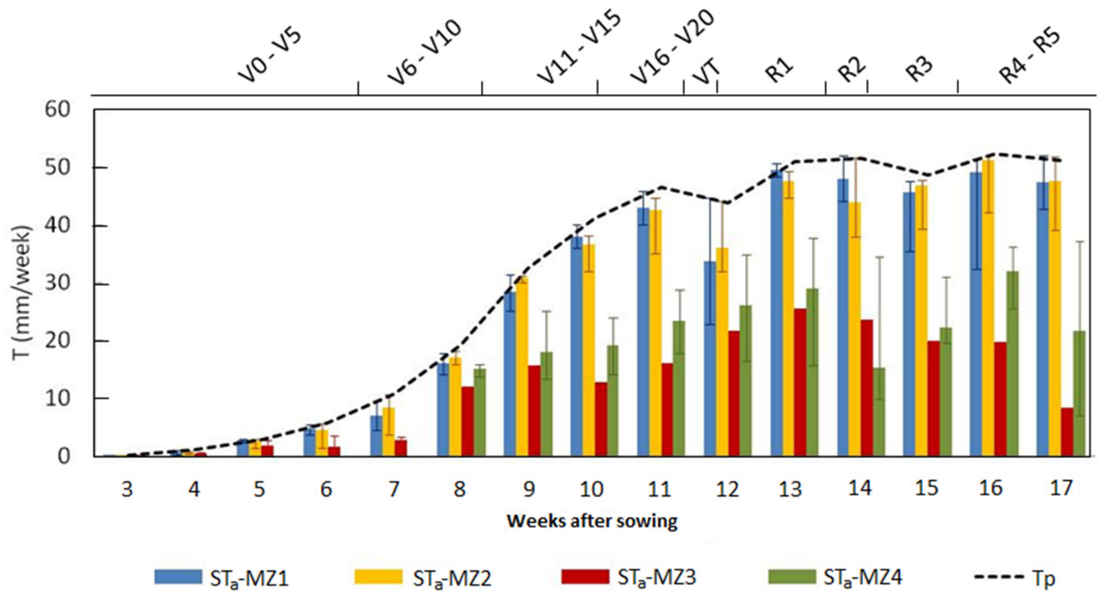

Figure 6. Simulated weekly transpiration at each MZ with the growing stages. Error bars represent the maximum and minimum and the dash line shows the weekly potential transpiration.

Tables

Table 1. Soil samples texture, Organic Matter (OM) and bulk density (ρ_b) averages at each station.

Station	Depth (cm)	D<0.002 mm Clay (%)	0.002<D<0.02 mm Fine Silt (%)	0.02<D<0.05 mm Coarse Silt (%)	0.05<D<2 mm Sand (%)	OM (%)	ρ_b (gr/cm^3)
P1	0 - 5	36	27.3	13.8	22.9	1.18	1.66
	5 - 35	32	33.6	14.5	19.9	0.71	1.63
	35 - 60	26.5	28.1	9.7	35.7	0.5	1.68
P2	0 - 5	25.9	26.4	14.8	32.9	1.59	1.57
	5 - 35	25.2	26.1	15.1	33.6	1.1	1.58
	35 - 60	24.2	23.4	14.7	37.7	0.98	1.59
P3	0 - 5	36.5	32.1	14.5	16.9	0.7	1.54
	5 - 35	21.3	27.8	16.7	34.2	0.5	1.65
	35 - 60	24.4	31.8	8.3	35.9	0.65	1.60
P4	0 - 5	28.7	23.6	13.2	34.5	2.71	1.48
	5 - 35	28.5	28.9	11	31.6	1.02	1.59
	35 - 60	28.6	19.8	10.4	41.2	1.14	1.60
P5	0 - 5	22.5	26.3	15.6	35.6	0.57	1.56
	5 - 35	28.9	36.6	20.3	14.2	0.72	1.58
	35 - 60	21.8	28.9	7.3	42.0	0.42	1.56
P6	0 - 5	29.9	26.9	15.1	28.1	2.11	1.64
	5 - 35	29.3	25.7	14.9	30.1	0.85	1.67
	35 - 60	30.2	26	14.8	29.0	0.7	1.69
P7	0 - 5	28.1	36	17.1	18.8	3.14	1.65
	5 - 35	28	27.8	11.9	32.3	1.48	1.72
	35 - 60	27.2	24.3	14.3	34.2	1.27	1.69
P8	0 - 5	25.7	28.7	15.2	30.4	2.22	1.58
	5 - 35	27.7	26.1	14.7	31.5	1.5	1.64
	35 - 60	29.2	27.3	14.7	28.8	1.02	1.78
P9	0 - 5	23.7	26.1	14.8	35.4	2.48	1.53
	5 - 35	23.6	27.8	14.4	34.2	1.06	1.51
	35 - 60	23.5	27.7	14.8	34	0.99	1.51
P10	0 - 5	27.7	25.8	20.3	26.2	1.84	1.61
	5 - 35	28.3	29.5	19.2	26.0	0.72	1.62
	35 - 60	24.6	33.5	9.5	32.4	0.81	1.80
P11	0 - 5	29.4	35.9	14.9	19.8	0.73	1.63
	5 - 35	30.3	34.7	14.9	20.1	0.5	1.65
	35 - 60	26.1	30.5	16.4	27.0	0.5	1.64

Table 2. Soil hydraulic parameters from each station, where: θ_s is the saturated water content; θ_r is the residual water content; α and n are shape parameters; K_s is the saturated hydraulic conductivity; θ_{fc} is simulated field capacity; and θ_{wp} is wilting point.

Station	Depth (cm)	θ_s ($cm^3 \cdot cm^{-3}$)	θ_r ($cm^3 \cdot cm^{-3}$)	α (cm^{-1})	n (-)	K_s ($cm \cdot d^{-1}$)	θ_{fc} ($cm^3 \cdot cm^{-3}$)	θ_{wp} ($cm^3 \cdot cm^{-3}$)
P1	0 - 5	0.424	0.026	0.0169	1.140	2.05	0.345	0.196
	5 – 35	0.407	0.027	0.0150	1.141	2.52	0.351	0.190
	35 - 60	0.364	0.037	0.0115	1.232	1.00	0.350	0.110
P2	0 - 5	0.389	0.061	0.0126	1.364	2.95	0.270	0.103
	5 – 35	0.388	0.060	0.0130	1.358	2.94	0.265	0.104
	35 - 60	0.321	0.047	0.0242	1.354	1.53	0.290	0.124
P3	0 - 5	0.418	0.012	0.0103	1.313	4.42	0.330	0.085
	5 – 35	0.362	0.025	0.0101	1.329	5.63	0.273	0.070
	35 - 60	0.341	0.017	0.0083	1.345	11.47	0.261	0.066
P4	0 - 5	0.439	0.024	0.0658	1.301	5.70	0.340	0.187
	5 – 35	0.400	0.031	0.0143	1.290	4.60	0.300	0.192
	35 - 60	0.395	0.018	0.0424	1.315	4.90	0.315	0.181
P5	0 - 5	0.450	0.062	0.0099	1.497	6.88	0.340	0.070
	5 – 35	0.460	0.067	0.0094	1.402	1.94	0.340	0.080
	35 - 60	-	-	-	-	-	-	-
P6	0 - 5	0.420	0.030	0.0126	1.153	12.00	0.371	0.172
	5 – 35	0.430	0.050	0.0828	1.154	9.40	0.390	0.198
	35 - 60	0.421	0.010	0.0974	1.146	8.10	0.390	0.182
P7	0 - 5	0.375	0.024	0.0105	1.118	1.06	0.300	0.208
	5 – 35	0.349	0.026	0.0380	1.141	3.34	0.300	0.196
	35 - 60	0.361	0.049	0.0391	1.141	4.10	0.280	0.107
P8	0 - 5	0.402	0.040	0.0135	1.375	4.01	0.310	0.123
	5 – 35	0.379	0.030	0.0115	1.356	3.05	0.280	0.090
	35 - 60	0.328	0.020	0.0121	1.287	1.75	0.280	0.080
P9	0 - 5	0.420	0.060	0.0105	1.462	5.79	0.300	0.089
	5 – 35	0.430	0.060	0.0107	1.441	4.70	0.330	0.091
	35 - 60	0.430	0.060	0.0109	1.433	5.52	0.330	0.090
P10	0 - 5	0.389	0.073	0.0115	1.421	3.98	0.301	0.105
	5 – 35	0.387	0.072	0.0112	1.425	4.56	0.300	0.080
	35 - 60	0.320	0.058	0.0181	1.256	1.87	0.290	0.090
P11	0 - 5	0.400	0.012	0.0784	1.121	10.00	0.380	0.188
	5 – 35	0.451	0.018	0.0308	1.141	5.27	0.375	0.188
	35 - 60	0.420	0.014	0.0121	1.112	11.00	0.350	0.250

Table 3. Periods where one or more stations change MZ membership.

Period (Day after sowing)	MZ1	MZ2	MZ3	MZ4
Period 1 (19-29)	P8, P9, P10	P1, P2, P3, P4, P5, P6	P7, P11	-
Period 2 (30-44)	P8, P9, P10	P1, P2, P3, P4, P5	P6, P7, P11	-
Period 3 (45-49)	P8, P10	P2, P3, P4, P5, P9	P1, P6, P7, P11	-
Period 4 (50-54)	P8, P10	P2, P3, P4, P9	P7, P11	P1, P5, P6
Period 5 (55-115)	P8, P10	P2, P3, P4, P5, P9	P11	P1, P6, P7

Table 4. Irrigation scheduling calendar based on growing stages and MZs distribution. h_{th}, is the possible pressure head threshold (the optimal pressure head threshold in bold); I, is the irrigation required to maximize transpiration; τ, is the irrigation duration; Z_{tr}, is the trigger soil depth. Optimal irrigation scheduling is represented in bold.

		V0-V5		**V6-V10**		**V11-V15**		**VT**		**R1-R6**	
		Trigger Depth = 10 cm		**Trigger Depth = 20cm**		**Trigger Depth = 20 cm**		**Trigger Depth = 40 cm**		**Trigger Depth = 40 cm**	
	h_{th} (kPa)	**Irrig. Required (mm)**	**τ (h)**	**Irrig. Required (mm)**	**τ (h)**	**Irrig. Required (mm)**	**τ (h)**	**Irrig. Required (mm)**	**τ (h)**	**Irrig. Required (mm)**	**τ (h)**
MZ1	**0**	-	-	-	-	-	-	-	-	-	-
	-10	-	-	-	-	-	-	-	-	-	-
	-20	-	-	-	-	-	-	-	-	-	-
	-23.3	-	-	**12.5**	**1.9**	-	-	-	-	-	-
	-26.7	**13.1**	**2.0**	13.5	2.1	-	-	-	-	-	-
	-30	14.0	2.2	14.1	2.2	**19.0**	**2.9**	**15.0**	**2.3**	**17.0**	**2.6**
	-40	15.0	2.3	14.5	2.2	21.0	3.2	17.0	2.6	21.0	3.2
	-60	16.0	2.5	18.5	2.8	25.0	3.8	23.0	3.5	29.0	4.5
	-100	17.1	2.6	22.5	3.5	29.0	4.5	33.0	5.1	45.0	6.9
	h_{th} (kPa)	**Irrig. Required (mm)**	**τ (h)**	**Irrig. Required (mm)**	**τ (h)**	**Irrig. Required (mm)**	**τ (h)**	**Irrig. Required (mm)**	**τ (h)**	**Irrig. Required (mm)**	**τ (h)**
MZ2	**0**	-	-	-	-	-	-	-	-	-	-
	-10	-	-	-	-	-	-	-	-	-	-
	-18.3	**12.4**	**1.9**	-	-	-	-	-	-	-	-
	-20	12.4	1.9	-	-	-	-	-	-	-	-
	-24	12.9	2.0	**15.3**	**2.4**	-	-	-	-	-	-
	-30	13.9	2.1	18.3	2.8	**13.0**	**2.0**	**13.0**	**2.0**	**13.0**	**2.0**
	-40	14.4	2.2	19.3	3.0	18.0	2.8	23.0	3.5	23.0	3.5
	-60	16.9	2.6	24.3	3.7	23.0	3.5	33.0	5.1	33.0	5.1
	-100	19.9	3.1	30.3	4.7	29.0	4.5	45.0	6.9	45.0	6.9

	h_{th} (kPa)	Irrig. Required (mm)	τ (h)	Irrig. Required (mm)	τ (h)	Irrig. Required (mm)	τ (h)	Irrig. Required (mm)	τ (h)	Irrig. Required (mm)	τ (h)
	0	-	-	-	-	-	-	-	-	-	-
	-10	-	-	**13.0**	**2.0**	**13.0**	**2.0**	**13.0**	**2.0**	**13.0**	**2.0**
MZ3	**-20**	**13.0**	**2.0**	17.0	2.6	17.0	2.6	21.0	3.2	21.0	3.2
	-30	15.0	2.3	21.0	3.2	21.0	3.2	29.0	4.5	29.0	4.5
	-40	16.0	2.5	23.0	3.5	23.0	3.5	33.0	5.1	33.0	5.1
	-60	18.0	2.8	27.0	4.2	27.0	4.2	41.0	6.3	41.0	6.3
	-100	20.5	3.2	28.0	4.3	28.0	4.3	43.0	6.6	43.0	6.6

	h_{th} (kPa)	Irrig. Required (mm)	τ (h)	Irrig. Required (mm)	τ (h)	Irrig. Required (mm)	τ (h)	Irrig. Required (mm)	τ (h)	Irrig. Required (mm)	τ (h)
	0	-	-	-	-	-	-	-	-	-	-
	-10	-	-	-	-	-	-	**13.0**	**2.0**	**13.0**	**2.0**
MZ4	**-16.7**	-	-	-	-	**15.0**	**2.3**	15.0	2.3	15.0	2.3
	-20	-	-	-	-	16.0	2.5	17.0	2.6	17.0	2.6
	-30	-	-	-	-	19.0	2.9	25.0	3.8	25.0	3.8
	-40	-	-	-	-	21.0	3.2	29.0	4.5	29.0	4.5
	-60	-	-	-	-	23.0	3.5	33.0	5.1	33.0	5.1
	-100	-	-	-	-	29.0	4.5	45.0	6.9	45.0	6.9

Table 5. Comparisons of optimal actual transpiration (OpT_a), optimal water applied ($OpIA$), simulated actual transpiration (ST_a), and simulated water applied (SAI).

	OpT_a (mm)	$(OpT_a - ST_a)/ST_a$ (%)	$OpIA$ (mm)	$(OpIA - SAI)/SAI$ (%)
MZ1	405.6	8.0	525.5	-11.0
MZ2	405.6	4.8	517.8	-12.8
MZ3	107.5	23.9	217.5	-28.5
MZ4	271.7	52.6	350.2	-16.6

Appendix A. Supplementary data

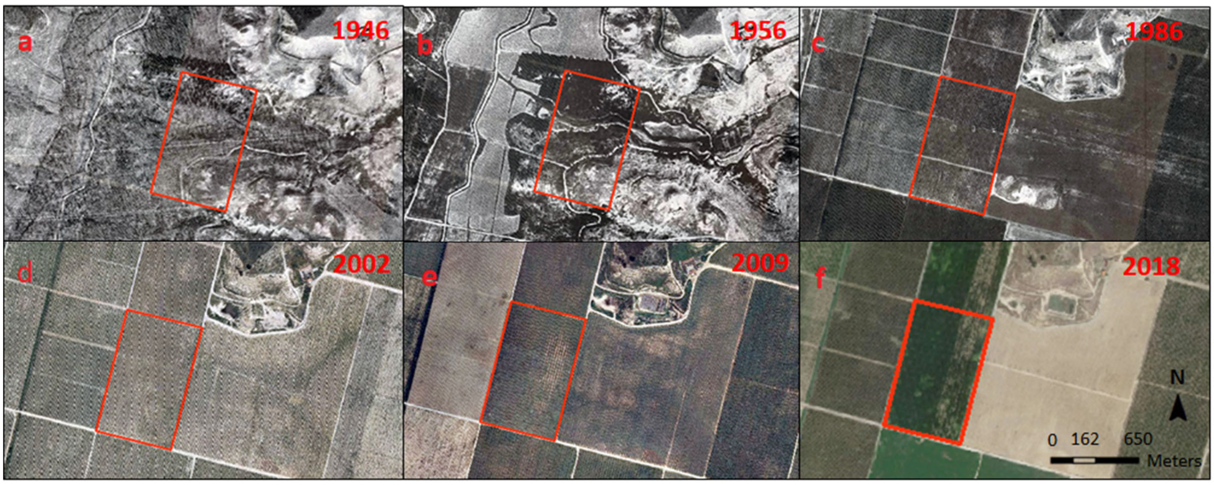

Figure A.1. Historical land use and topography modifications at the study site.

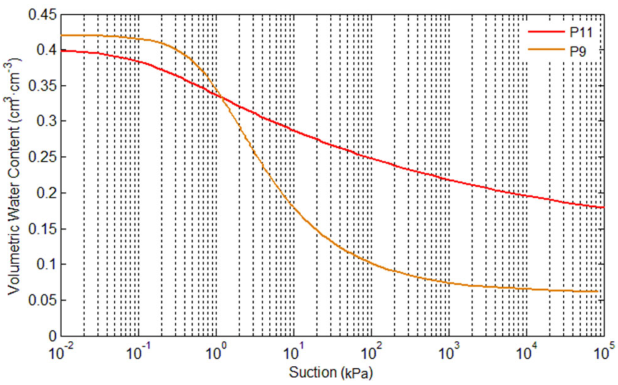

Figure A.2. Soil water retention curves at 10 cm depth from two stations located on opposite edges of the filed. Station P9 is located on the west side and P11 on the east.

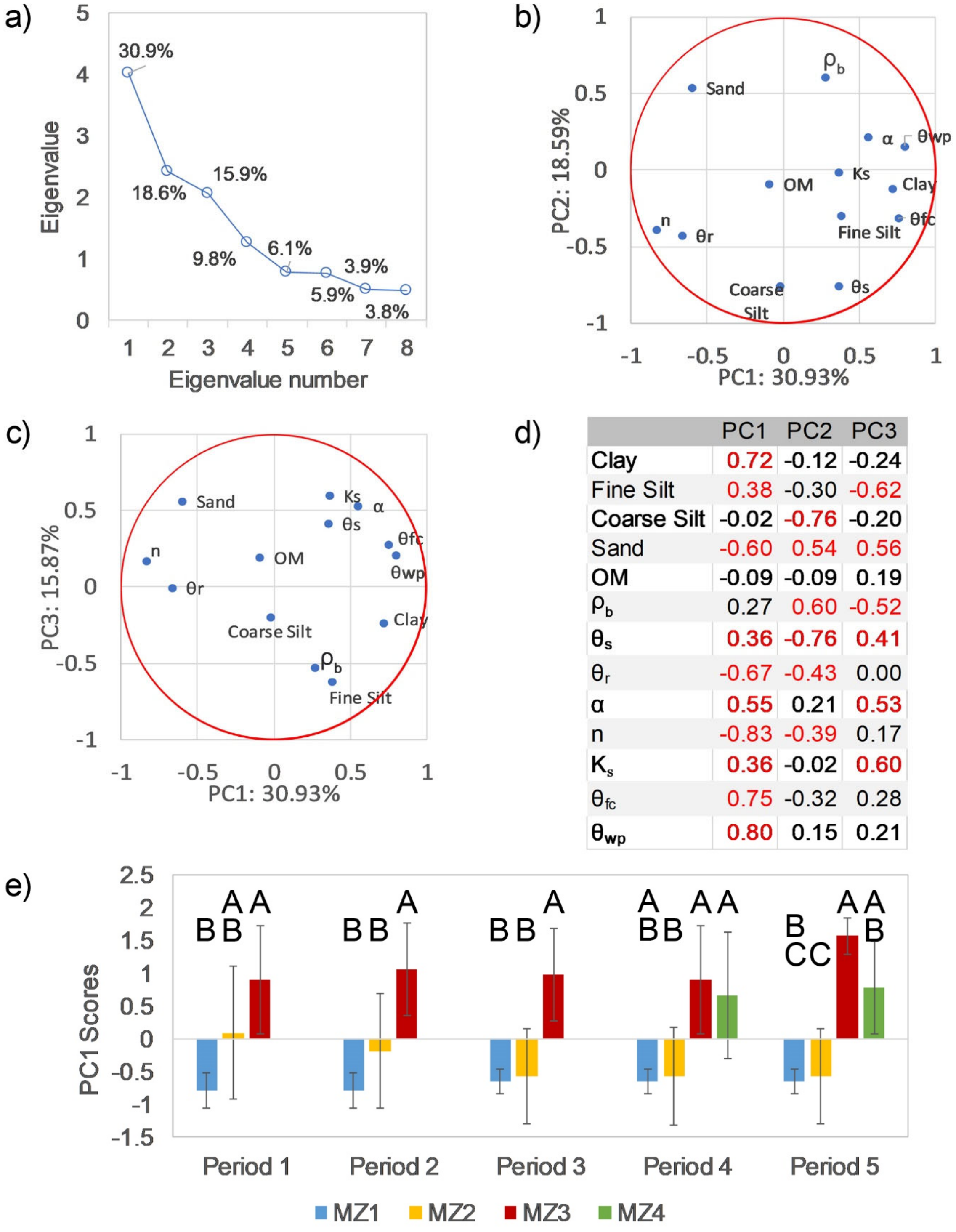

	PC1	PC2	PC3
Clay	0.72	-0.12	-0.24
Fine Silt	0.38	-0.30	-0.62
Coarse Silt	-0.02	-0.76	-0.20
Sand	-0.60	0.54	0.56
OM	-0.09	-0.09	0.19
ρ_b	0.27	0.60	-0.52
θ_s	0.36	-0.76	0.41
θ_r	-0.67	-0.43	0.00
α	0.55	0.21	0.53
n	-0.83	-0.39	0.17
K_s	0.36	-0.02	0.60
θ_{fc}	0.75	-0.32	0.28
θ_{wp}	0.80	0.15	0.21

Figure A.3. a) Eigenvalue and percent of variance explained by the first eight components of the principal component (PC) analysis; b) bi-plot of select soil properties (clay, fine silt, coarse silt, sand, and organic matter (OM) content; bulk density (ρ_b); water content at saturation (θ_s); residual water content (θ_r); water content at field capacity (θ_{fc}); water content at wilting point (θ_{wp}); saturated hydraulic conductivity (K_s); and shape parameters α and n) for PC1 and PC2; c) same for PC1 and PC3; d) Pearson correlation matrix for the first three PCs and selected soil properties (significant ($p<0.05$) correlations highlighted in red); and e) averages (bars) and standard deviations (lines) of PC1 for the four management zones (MZs) through the growing season. Capital letters indicate significant ($p<0.05$) differences within MZs according to the Kruskal-Wallis test.